Molecular dynamics investigations of the coalescence of iron clusters embedded in an inert-gas heat bath

N. Lümmen and T. Kraska*
Physical Chemistry, University of Cologne, Luxemburger Strasse 116, D-50939 Köln, Germany
(Received 27 July 2004; revised manuscript received 28 October 2004; published 13 May 2005)

A detailed analysis of the coalescence of iron clusters over the course of their growth in an inert-gas atmosphere is presented. The investigation is performed by molecular dynamics simulations, using a recent version of the embedded atom method for iron. For several coalescence events extracted from realistic particle-growth simulations, the change of temperature, the atomic structure, and the morphology are analyzed. Here, the change in morphology is investigated by the relative number of atoms in the surface related to the driving force of the coalescence, the surface energy. The duration of the coalescence depends on the state of the colliding clusters, which is related to their temperature. At elevated temperatures an exponential decay of the relaxation of the cluster shape is found in case of liquid clusters. Clusters at lower temperatures exhibit a regular atomic structure. The coalescence includes the restructuring of the clusters, leading to deviations from the exponential decay of the cluster properties. Here, a distinct three-step coalescence process has been identified for structured clusters under nonadiabatic conditions. Each of these steps is related to a different extent of heat exchange with the carrier gas.

DOI: 10.1103/PhysRevB.71.205403 PACS number(s): 61.46.+w, 64.70.Nd, 81.05.Bx, 81.07.Bc

I. INTRODUCTION

Coalescence is an important growth mode in particle-formation processes, for example, in inert-gas aggregation sources (IGA). It significantly affects the morphology of the particles. In this context the exchange of heat between the particles and the environment is important. This heat makes it possible to reorganize the atomic structure in a cluster. The detailed knowledge of the cluster coalescence contributes to the understanding of the resulting particle properties and provides information on how to influence a process in order to obtain desired properties.

Although there is an increasing interest towards understanding the structure and the properties of metal particles, so far a few theoretical investigations of the formation process of nanoparticles from the supersaturated gas phase have been published. There are several investigations of the structure and energy of different clusters.[1–3] They are often restricted to the structural ground state, omitting excited states, which are actually present over the course of a real particle-formation process. Furthermore, often the magic number clusters are investigated, which are known to be more stable than other clusters from experimental investigations. These magic number clusters have been found with a higher frequency than other cluster sizes, using mass spectrometry.[4,5] However, the total number of all nonmagic number clusters is larger than the number of magic number clusters. It is unlikely that two colliding clusters have both filled shells at the moment of the collision. Therefore, it is important to include the analysis of others rather than these idealized clusters in the examination of the growth process. Investigations of specific selected cluster structures do not usually account for the effect of supersaturation or the presence of a carrier gas. In order to analyze these influences, the coalescence processes, which happen during the cluster formation from the gas phase, have to be investigated.

There are several molecular dynamics (MD) studies of the coalescence of small clusters. Zhao *et al.*,[6] for example, investigated the coalescence of three identical, perfectly icosahedrally structured silver clusters using an analytical embedded-atom-method (EAM) potential. In the simulation of this symmetric three-body collision, which is a rather unlikely event, a homogeneous MD thermostat was used, neglecting differences in heat removal from the core and the surface of the cluster. The aspect ratio of the cluster was chosen as the order parameter, estimating the morphological changes over the course of the coalescence process. With a similar embedded-atom-method molecular-dynamics (EAMMD) method, using a homogeneous thermostat, the coalescence of gold clusters of different selected sizes was investigated.[7] In that work the radius of gyration was used in addition to the aspect ratio for describing the shape of the clusters. As a result it was found that the macroscopic models for sintering by surface diffusion fail to describe the coalescence of small clusters. In further investigations of the coalescence of small lead clusters[8] an empirical glue potential including many-body interactions was employed. Due to the low number of collisions with inert-gas atoms at the chosen carrier gas pressures the authors argued that constant energy simulations are a good approximation. Therefore only constant energy simulations were performed. The temperature and the aspect ratio were investigated during the coalescence of two perfect 565-atom clusters with a given icosahedral structure. Three types of coalescence were identified: solid-solid coalescence by diffusion resulting in highly defective clusters, liquid-liquid coalescence, and melting during coalescence followed by cooling down and solidification. Zachariah and Carrier[9] have investigated the sintering of silicon nanoparticles modeled by the many-body Stillinger-Weber potential.[10] For the simulation of the sintering process a constant energy ensemble was used after equilibrating the system at a chosen temperature with a constant-temperature

simulation method. The moment of inertia was used as an order parameter for the sphericity of the newly formed cluster. A continuous sintering from the first encounter of the two clusters over a dumbbell and a change from an oval shape to a spherical shape was observed within 4 ns simulation time for a 480-atom cluster. More recently Lehtinen and Zachariah[11] developed an analytical model including the formation of heat during the coalescence process as well as the heat removal by collisions with a carrier gas. As a result they found that the particle temperature can be several hundred degrees above that of the carrier gas, as found experimentally.[12] When increasing the temperature by a few degrees, a transition from a slow coalescence to a 1- to 3-orders-of-magnitude accelerated coalescence was observed.

In recent investigations we have analyzed the growth process of iron clusters from a supersaturated gas phase[13] by molecular dynamics simulations. In addition the effect of the amount of carrier gas on the growth process has also been analyzed.[14] Over the course of the growth process both surface growth and the coalescence of clusters take place. Since coalescence is a stochastic process that requires the collision of two clusters moving in space, it is not possible in advance to define a specific time or cluster temperature at which the collision happens. Therefore, in contrast to other investigations in the literature, we analyze here the realistic coalescence processes that happen during cluster growth simulations for different carrier-gas temperatures and amounts.

II. METHOD

We employ the molecular dynamics (MD) simulation method for the investigation of coalescence dynamics. Within this method the Newton equations of motion are solved numerically for each atom in the force field of all other atoms. In order to treat clusters with several hundred to a few thousand atoms we use the embedded atom method (EAM) for modeling the force field acting between the atoms. This commonly used force field for metals consists of two contributions: a multibody term describing the contribution to the energy by the delocalized electrons and a term for the pairwise additive interaction of the atomic cores,[15–17]

$$E_i = F_i[\rho_i] + \frac{1}{2}\sum_{i,j\neq i} \phi_{ij}(r_{ij}). \tag{1}$$

Here ρ_i is the local electron density at the position of atom i, which can be calculated from the contributions of the atomic electron densities ρ_j^{at} of all surrounding atoms j,

$$\rho_i = \sum_{j\neq i} \rho_j^{at}(r_{ij}). \tag{2}$$

The contribution of each atom to the electron density at the position of a certain atom is calculated from the functions of Clementi and Roetti[18] for the 4*s* and the 3*d* orbitals. The pairwise interaction of the atomic cores is modeled by a screened Coulomb potential,

$$\phi_{ij}(r_{ij}) = \frac{Z_i(r_{ij})Z_j(r_{ij})}{r_{ij}}, \tag{3}$$

with effective charges $Z(r_{ij})$, which are fitted together with the multibody functional $F_i[\rho_i]$ to the experimental data of the elastic constants, the sublimation energy, and the vacancy-formation energy.[15–17,19] Here, we employ a version of the EAM developed for bcc iron and its alloys.[19] The suitability of this model for the investigation of the properties of iron nanoparticles has been discussed in earlier papers.[13,14]

For the thermalization of the clusters before and after a collision, a heat bath consisting of an inert gas is added. Within this method the substance under investigation is thermalized only by collisions with atoms of an inert gas such as argon. Since the monoatomic argon atoms do not condense under given conditions, they can be treated by a regular homogeneous MD gas-phase thermostat.

For the analysis of the atomic structure of the cluster we use the common-neighbor analysis (CNA).[20–22] With the CNA one can identify the structural environment of each atom by a systematic geometric analysis of the neighborhood of the atom. The result of this analysis is a set of three-digit signatures that can be used to identify the structure. Here, we take into account four structure types. These are the close-packed structures fcc and hcp, the bcc, and the icosahedral structures. All substructures such as bulk, surface, or edge atoms are summarized in the corresponding main structure type. Ambiguous structures are not accounted for. Hence, all atoms counted are in the specific structure, while it is possible that some unidentified atoms might be also in one of the four types of structures mentioned above, within the uncertainty of the method. In addition it should be mentioned that the fcc and hcp structures are both close-packed structures, differing only in the sequence of the layers. Hence differences in fcc and hcp structures can be caused by stacking faults, and therefore both structures are summarized as close-packed structures.

The morphology of the particles is analyzed by the surface fraction, which is defined as the ratio of the number of atoms in the surface to the number of all atoms in a cluster,

$$x_{\mathrm{surf}} = \frac{N_{\mathrm{surf}}}{N_{\mathrm{cluster}}}. \tag{4}$$

The atoms in the surface of a cluster are identified by the cone algorithm.[23] The lowest surface fraction is given for spherical clusters, while nonspherical clusters or clusters with a rough surface have a higher surface fraction. The minimum value of the surface fraction for a given number of atoms in the cluster is estimated here as a reference from the equations for spherical fcc clusters.[24] The number of atoms in a cluster N_{cluster} as a function of the number of shells N_{sh} is given by

$$N_{\mathrm{cluster}} = \frac{10}{3}N_{\mathrm{sh}}^3 - 5N_{\mathrm{sh}}^2 + \frac{11}{3}N_{\mathrm{sh}} - 1. \tag{5}$$

The number of surface atoms as a function of the number of shells is given by

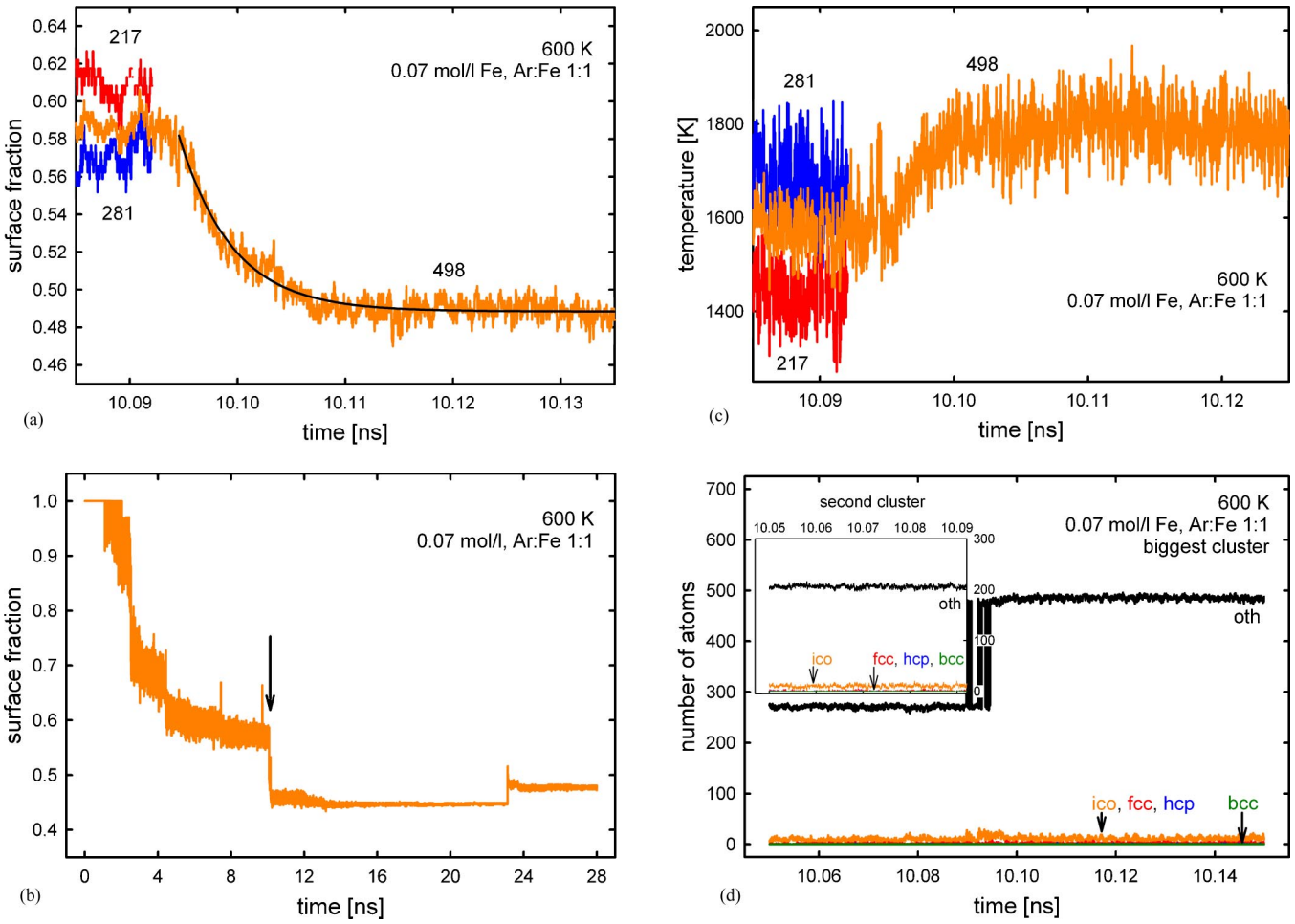

FIG. 1. (Color online) Results for the coalescence process *C*1. The corresponding conditions are given in Table I: (a) The development of the surface fraction of the two clusters before and after the collision. The numbers indicate the number of atoms in the clusters. In addition the size-averaged surface fraction before the collision is shown. The curve is the fitted to an exponential decay function with the parameter set given in Table I. (b) The surface fraction over the time period of the complete simulation. The increasing surface fraction at about 23 ns is related to an agglomeration process, leading to an agglomerated shape with a high surface fraction. The arrow marks the event shown in (a). (c) The temperature of the clusters and (d) common neighbor analysis of the clusters before and after the collision.

$$N_{\mathrm{surf}} = 10N_{\mathrm{sh}}^2 - 20N_{\mathrm{sh}} + 12. \tag{6}$$

In order to calculate the surface fraction continuously we first calculate the number of shells N_{sh} for a given number of atoms in the cluster N_{cluster} and then insert the resulting N_{sh} in the equation for the number of surface atoms N_{surf}. This theoretical minimum value of the surface fraction for a given number of atoms cannot usually be reached. One reason is that the minimum surface fraction is a continuous interpolation of the values for distinct magic-number clusters. Furthermore, fluctuations at the cluster surface lead to a larger surface fraction.

The driving force of the coalescence is the minimization of the surface energy by minimizing the cluster surface area. Therefore, the coalescence process can be modeled by the following linear differential equation:[25]

$$\frac{da}{dt} = -\frac{a - a_{\mathrm{end}}}{\tau}. \tag{7}$$

Here a is the surface of the cluster and a_{end} is the surface of the cluster with the same number of atoms at the end of the coalescence process. Ideally the latter one corresponds to the surface fraction of a spherical cluster. With $x_{\mathrm{surf}} = N_{\mathrm{surf}}/N_{\mathrm{cluster}}$ one can replace a by x_{surf} and obtain after integration

$$x_{\mathrm{surf}} = x_{\mathrm{end}} + \delta x \exp\left(-\frac{t - t_{\mathrm{start}}}{\tau}\right). \tag{8}$$

Here, t_{start} is the time when the coalescence starts, and δx is a pre-exponential parameter describing the range of the surface-fraction change during coalescence. At $t = t_{\mathrm{start}}$ one obtains $x_{\mathrm{start}} = x_{\mathrm{end}} + \delta x$. Hence, one can insert the initial value of x_{surf} into Eq. (8),

$$x_{\mathrm{surf}} = x_{\mathrm{end}} + (x_{\mathrm{start}} - x_{\mathrm{end}})\exp\left(-\frac{t - t_{\mathrm{start}}}{\tau}\right). \tag{9}$$

The kinetic temperature of the clusters is calculated from the velocity of the atoms in the clusters, corrected by the motion of the complete clusters. During the growth the biggest cluster in the system undergoes 5–10 coalescence and/or agglomeration processes with other medium-to-large-sized

TABLE I. Fitted parameters of Eq. (8) for different coalescence events. t_{start}: moment at which the collided clusters never separate again. x_{end}: parameter of Eq. (8), surface fraction at the end of the coalescence process. x_{sphere}: minimum surface fraction of a spherical cluster with the same number of atoms as after the collision. $\delta x = x(t_{start}) - x_{end}$. τ: time constant of the exponential decay of the surface fraction. x_{sim}: surface fraction at the end of the simulation or before another collision event happens

ρ (mol dm^{-3})	T(Ar) (K)	Ar:Fe	$N_1+N_2=N$	t_{start} (ns)	x_{end}	x_{sphere}	δx	τ (ps)	x_{sim}	Event no.
0.07	600	1:1	281+217=498	10.09456	0.488428	0.463628	0.093467	4.932	0.485743	*C*1
0.07	800	1:1	397+284=681	16.23508	0.473778	0.426361	0.047827	4.709	0.454545	*C*2-neck
0.07	800	1:1	397+284=681	16.23508	0.454545	0.426361	0.067060	132.1	0.454545	*C*2-oval
0.05	1000	3:1	203+140=343	13.38752	0.551020	0.510642	0.069980	4.545	0.555728	*C*3
0.02	600	3:1	117+89=206	15.67801	0.616949	0.578865	0.071884	3.091	0.601426	*C*4
0.02	800	3:1	135+77=212	15.39482	0.612361	0.574923	0.0805407	3.331	0.611229	*C*5
0.02	800	5:1	131+107=238	14.46228	0.579832	0.559148	0.1092440	9.273	0.578554	*C*6
0.02	800	10:1	139+68=207	10.52935	0.615357	0.578199	0.062802	3.184	0.592740	*C*7
0.02	800	5:1	239+23=262	15.3892	0.568702	0.546190	0.038168	2.667	0.568467	*C*8
0.02	600	10:1	86+61=147	8.47214	0.653061	0.652850	0.095238	9.081	0.659852	*C*9

clusters. After the particle formation in the simulation box is completed the temperature of the cluster approaches the temperature imposed on the inert-gas phase. All of the properties mentioned above have been analyzed for several representative coalescence processes in the carrier-gas medium taken from cluster growth simulations. The examples cover different cluster sizes, temperatures, and process types.

III. RESULTS

In Fig. 1 the surface fraction, temperature, and CNA of two clusters before and after a collision are shown. This coalescence process corresponds to the event *C*1 in Tables I and II. In addition, the weighted average surface fraction and the temperature of the two clusters before the collision are plotted. Figure 1(a) shows that at the onset of the coalescence the surface fraction starts to decrease. This corresponds to the relaxation of the cluster shape towards a spherical shape. The resulting cluster is bigger than the two clusters prior to the collision, and the surface fraction has to be smaller. The relaxation of the surface fraction is correlated with the exponential decay function [Eq. (8)] and plotted in the diagram. Due to the definition of a cluster by the Stillinger criterion[26] and the relative movement of the two clusters, it can happen that the system fluctuates between the states of two separated clusters and one big cluster for a short period of time. The onset of the coalescence is defined here as the time of the last contact after which the cluster does not fall apart anymore. We fix this value for t_{start} and the corresponding surface fraction x_{start} as well as x_{end}, and we obtain the relaxation constant τ by the correlation of the time-dependent surface fraction with Eq. (8). The decay of the surface fraction follows the exponential function perfectly. Figure 1(d) shows that the two colliding clusters do not contain a significant amount of ordered structure. The surface

TABLE II. Collision parameters and temperature change over the course of the coalescence. r_i: radius of the cluster. b: collision parameter. α: angle between velocity vectors before initial contact of the collision partners. $T_{av,sim}$: weighted average temperature of the collision partners before collision, as calculated from simulation data. $T_{nc,sim}$: temperature of the newly formed cluster after the postcollision temperature increase, as estimated from the temperature plot. ΔT_{sim}: increase of the cluster temperature after the collision, as estimated from the temperature plots. ΔT_{th}: theoretical increase of cluster temperature after collision due to number of particles of the collision partners. See Eq. (10) for details. $T_{m,th}$: theoretical melting point of the newly formed cluster. See Eq. (11) for details.

r_1 (Å)	r_2 (Å)	$\frac{b}{(r_1+r_2)}$	N	b (Å)	α/°	$T_{av,sim}$ (K)	$T_{nc,sim}$ (K)	ΔT_{sim} (K)	ΔT_{th} (K)	$T_{m,th}$ (K)	Event no.
9.90	8.96	0.650	498	12.255	140.5	1600	1800	200	393	1740	*C*1
10.80	9.66	0.154	681	3.158	158.9	930	1100	170	367	1746	*C*2
8.69	7.69	0.272	343	4.459	64.2	1030	1250	220	456	1732	*C*3
7.27	6.696	0.908	206	12.687	120.8	1280	1500	220	538	1720	*C*4
7.707	6.41	0.523	212	7.385	106.5	1500	1800	300	508	1721	*C*5
7.54	7.068	0.433	238	6.32	155.8	1050	1400	350	519	1723	*C*6
7.663	6.10	0.114	207	1.57	78.79	970	1170	200	515	1720	*C*7
9.199	4.40	0.952	262	12.94	104.84	1200	1350	150	283	1726	*C*8
6.57	5.908	0.039	147	0.49	99.5	850	1080	230	604	1711	*C*9

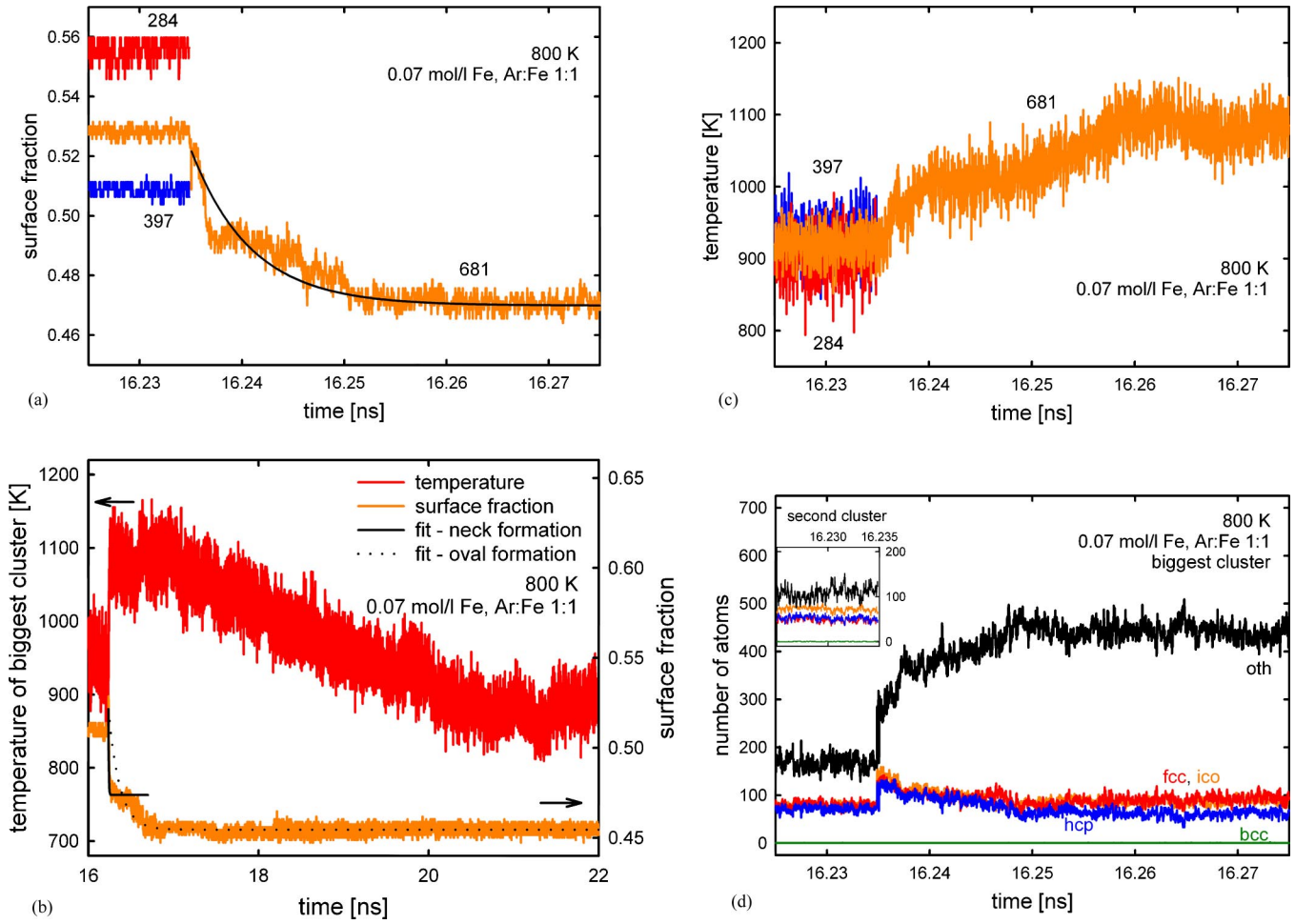

FIG. 2. (Color online) Results for the coalescence process *C*2. The corresponding conditions are given in Table I: (a) The surface fraction of the clusters before and after the collision (neck formation). (b) The surface fraction over a longer time period together with the cluster temperature. The solid curve is the exponential decay based on the first limiting value of the surface fraction at 0.4738, as shown in Fig. 2(a) (*C*2-neck in Table I). The dotted curve is the exponential decay with the limiting value of 0.4545 (*C*2-oval in Table I. (c) The temperature of the clusters. (d) Common neighbor analysis of the clusters.

fraction at 10.13 ns in Fig. 1(a) has a value of approximately 0.488 and decreases to 0.486 [Fig. 1(b)]. However, it does not reach the value corresponding to a spherical cluster, estimated by the magic-number clusters which is 0.46. The reason for this deviation is the roughness of the cluster surface, as mentioned above. In Fig. 1(c) the development of the temperature over the course of the coalescence is shown. Before the collision the smaller cluster (217 atoms) is cooled to approximately 1420 K, while the larger cluster is still at approximately 1700 K. The atom-number weighted temperature of both clusters is around 1600 K. During coalescence the temperature of the resulting cluster increases to about 1800 K. One can also see that the temperature remains approximately constant over a small period of time after the coalescence. This also shows that the collisions with the carrier-gas atoms do not have a significant effect on the cluster temperature in the considered time interval of a few picoseconds. One can therefore consider this part of the coalescence process as quasiadiabatic.

In Fig. 2 a coalescence process of two clusters of comparable size is shown. In this case the temperatures of both clusters are approximately 930 K before the collision [Fig. 2(c)]. After the collision the temperature rises up to approximately 1080 K. However, the increase of the temperature as well as the decrease of the surface fraction shown in Fig. 2(a) do not follow the exponential decay function as closely as the coalescence process shown in Fig. 1. The CNA of this coalescence process is shown in Fig. 2(d). Both clusters contain a significant number of atoms that are in one of the solid structures. At the collision the number in each identified icosahedral and close-packed structure is about 130 to 140 atoms. The number of atoms in the nonidentified structure is about 290 atoms. After the collision the CNA shows a decreasing amount of regular structures and an increasing amount of disordered structures. The changes in surface fraction and temperature are related to each other. For example, at about 16.24 ns the surface fraction does not change much over a short time period during coalescence. When the coalescence process prolongs, the temperature remains constant. The surface fraction at 16.27 ns in Fig. 2(a) is significantly higher than the surface fraction after 28 ns, having a value of 0.4545 [Fig. 2(b)]. The value obtained from the interpolation

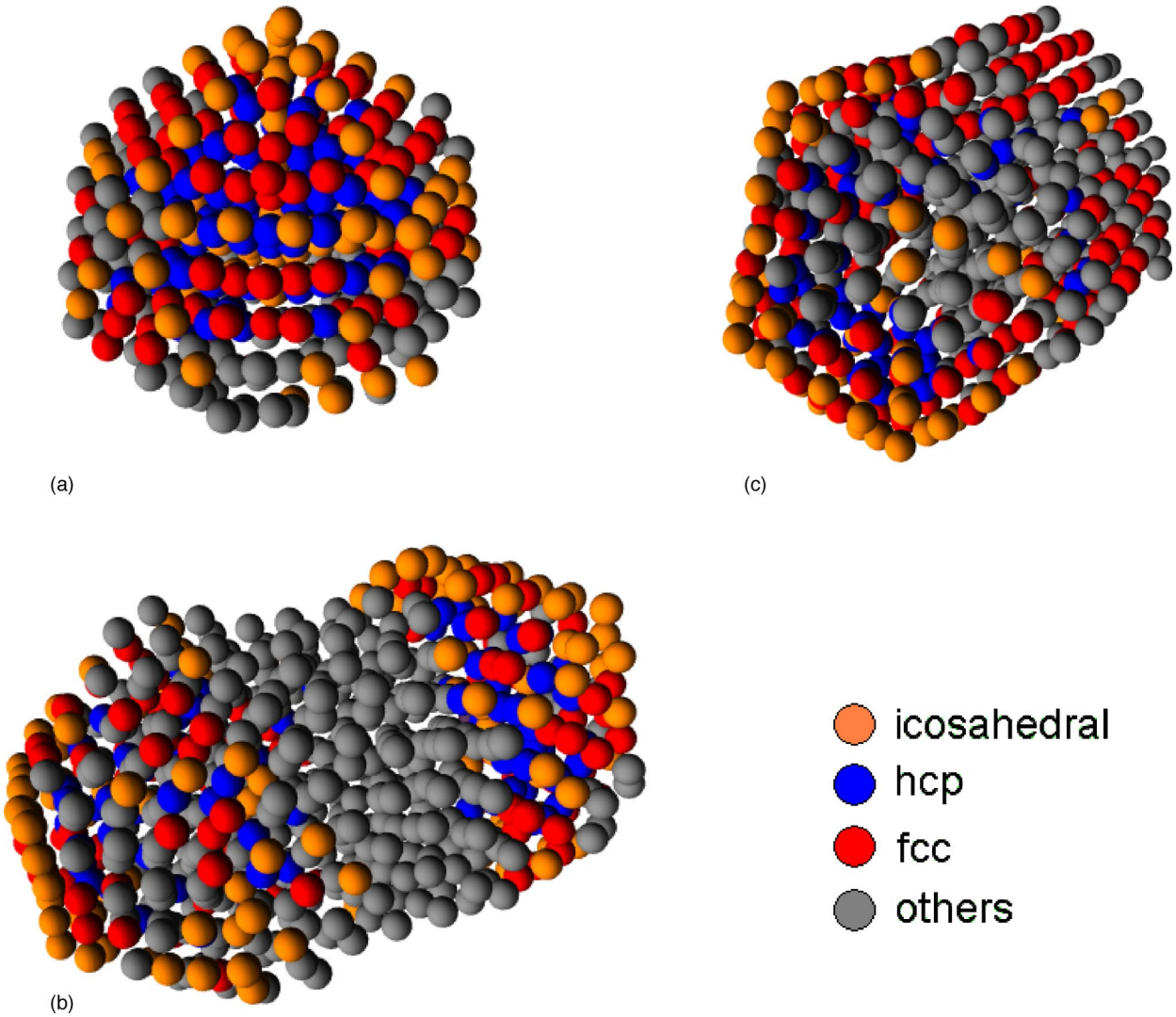

FIG. 3. (Color online) Snapshots of the cluster taken from process *C*2 (Fig. 2). (a) The biggest cluster before the collision. (b) The new cluster 0.165 ns after the collision or at 16.4 ns of the overall simulation time. (c) The cluster at 11.3 ns after the collision or 27.5 ns of the overall simulation time. The radii of the atoms in the snapshots are smaller than the real radii for better visibility.

of the spherical magic-number clusters is 0.4264 and hence significant below the value at the end of the simulation. In Fig. 3 snapshots are shown of the bigger cluster before the collision and the new cluster at 0.165 ns after the collision. While the bigger cluster is rather spherical and exhibits a structured domain before the collision, the new cluster is dumbbell-like, with structured domains at the end cups only after the collision. At the side of the collision the clusters lose their structure, which is related to the restructuring and diffusion of atoms into the neck region. In Fig. 3(c) the same cluster is shown 11.3 ns after the collision. It has changed into an elongated oval shape with some triangular facets. At this point a perfectly spherical shape is not reached yet. The obtained relaxation constant τ, representing the coalescence time, depends on the range of the surface fraction and the time period included in the correlation. The coalescence time for the first step with the limiting value 0.4738, as shown in Fig. 2(a), is in the order of a few picoseconds (5.8 ps). If the next step of the coalescence is included in the correlation using a limiting surface fraction of 0.4545 at 28 ns, the coalescence time is on the order of hundreds of picoseconds [132 ps, Fig. 2(b)]. It can be expected that the coalescence process continues from the oval to the spherical shape beyond the 28-ns simulation time. However, since the coalescence of a solid cluster is determined by surface diffusion, the relaxation constant of this final step for a given temperature is expected to be beyond the time scale of the molecular dynamics simulations performed here.

In Fig. 4 a similar coalescence process to that in Fig. 2 is shown, but for smaller clusters. It corresponds to event *C*3 listed in Tables I and II. One can observe a hold point at about 13.390–13.395 ns for the surface fraction [Fig. 4(a)] and the temperature [Fig. 4(c)]. The decay of the surface fraction does not perfectly follow an exponential decay function. The CNA in Fig. 4(d) supports the idea that the coalescence involves the restructuring of the clusters. The surface fraction at the end of the simulation at 20 ns has the value 0.5510, which differs from the value for the spherical shape. Figures 5 and 6, on the other hand, show the coalescence processes which follow the exponential decay function

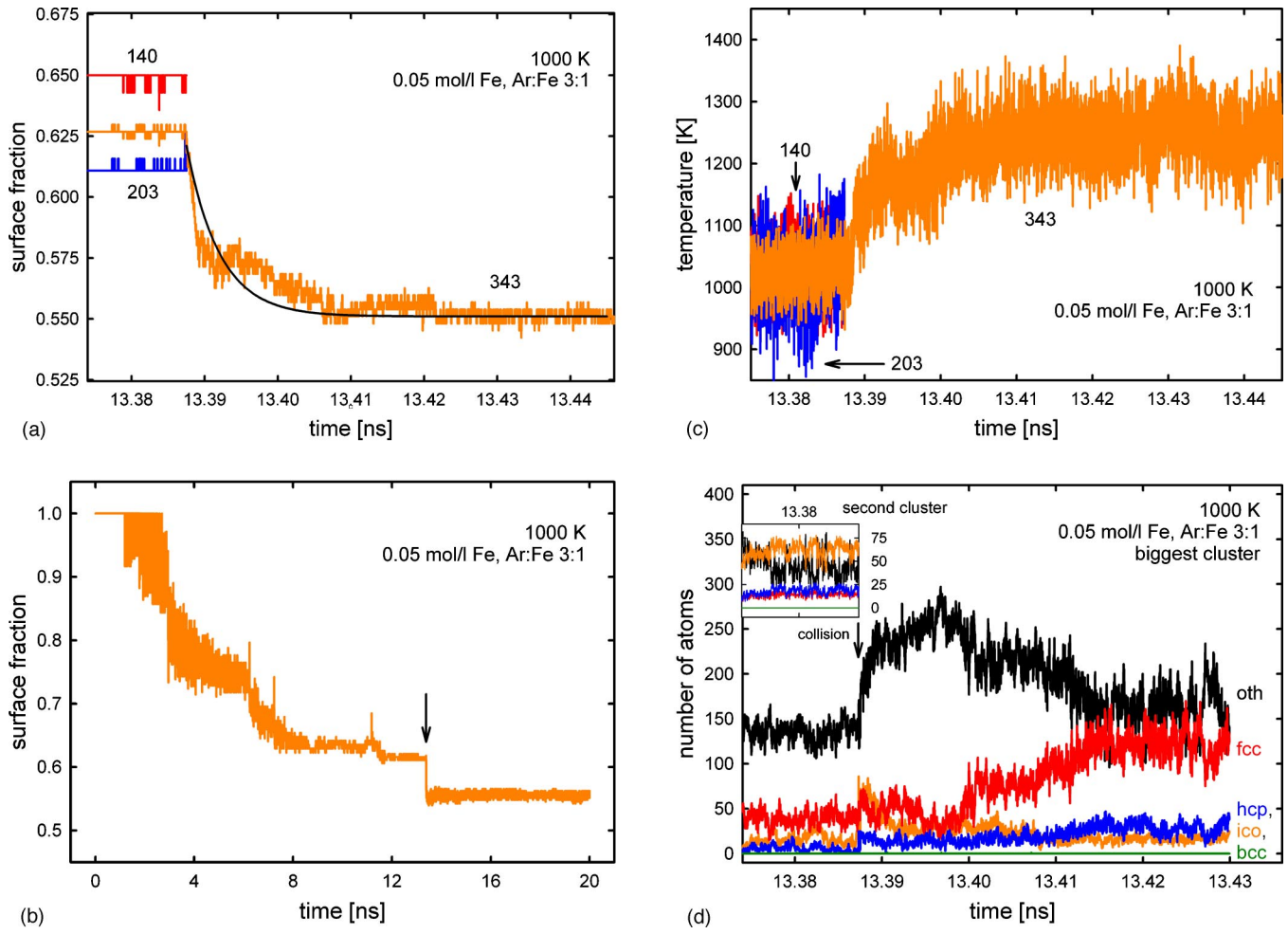

FIG. 4. (Color online) Results for the coalescence process *C*3. (a) the surface fraction of the clusters in high resolution. (b) The overall development of the surface fraction. The arrow marks the event shown in (a). (c) The temperature of the clusters and (d) common neighbor analysis of the clusters.

closely (events *C*4 and *C*5). Again the behavior of the decay of the surface fraction can be explained by the temperature of the clusters being related to their states. The clusters are liquid as indicated by the CNA presented in Figs. 5(d) and 6(d), and droplet coalescence takes place.

Hendy *et al.*[8] pointed out that a coalescence process of two solid particles is accelerated, if the temperature of the newly formed particle rises above its melting temperature. We have estimated the temperature increase due to coalescence with a formula given in that work,[8]

$$\Delta T = \frac{3\sigma}{\rho c_v}\frac{1}{R_2}\frac{[1+(R_1/R_2)^2]-[1+(R_1/R_2)^3]^{2/3}}{[1+(R_1/R_2)^3]}. \quad (10)$$

Here, temperature-dependent values for the surface tension σ and the density[27] ρ have been used, as well as the value of the heat capacity for the bulk phase c_v [449 J/(kg K)].[28] The cluster radii are calculated from the mean distance of the surface atoms from the center of mass. R_1 is always defined with the radius of the smaller particle. A comparison of the temperature increase as obtained from Eq. (10) and that observed in the simulation is listed in Table II. In general one can see that the predicted value obtained from Eq. (10) overestimates the temperature increase obtained in the simulation. Some possible sources for this difference are deviations of the bulk properties used in Eq. (10) from the corresponding properties of finite-size clusters. Also the impact of the collision influences the coalescence process. The magnitude of the impact is determined by the velocities of the clusters before the collision as well as the collision parameter and angle.

For calculating the melting temperature of the newly formed clusters, we use an equation given by Lewis *et al.*[7] based on bulk properties that gave reasonable results for gold nanoclusters,

$$T_m(R) = T_b\left(1 - 2\frac{\sigma_s - \sigma_l(\rho_s/\rho_l)^{2/3}}{\rho_s L R}\right). \quad (11)$$

Here, T_b is the bulk melting temperature for iron (1807 K), L is the heat of fusion (2.667 MJ/kg), R is the cluster radius, σ_s and σ_1 are the surface tensions of the solid and liquid phases (σ_s=2.44 J/m^2 and σ_1=1.788 J/m^2), and ρ_s and ρ_l are the densities of the corresponding phases (ρ_s=7.874 g/cm^3 and ρ_1=7.01 g/cm^3).[27,28] The estimated values for the melting temperatures of the clusters after the collisions are listed in

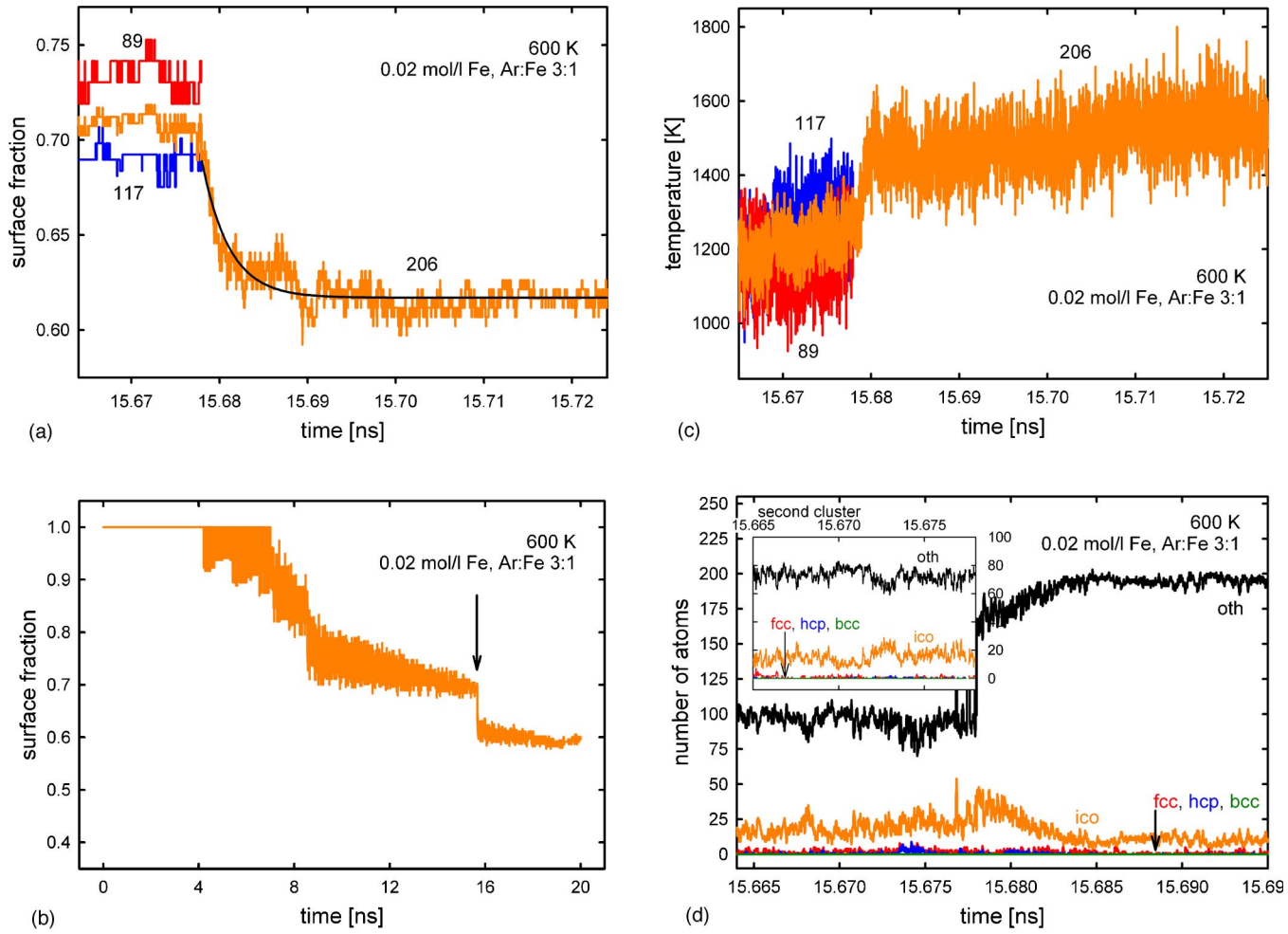

FIG. 5. (Color online) Results for the coalescence process *C*4. (a) The surface fraction of the clusters in high resolution. (b) The overall development of the surface fraction. The arrow marks the event shown in (a). (c) The temperature of the clusters and (d) common neighbor analysis of the clusters.

Table II. By comparison of the estimated melting temperature and the cluster temperature after the collision one can determine whether the cluster is liquid or solid. In the case of event *C*2 the temperature of the simulation is at 1100 K, whereas the estimated melting temperature is at 1746 K, suggesting a coalescence of solid clusters. This is in agreement with the discussion concerning the coalescence event above. In event *C*1 the cluster at 1800 K is clearly liquid, also being in agreement with the discussion above. In this case the coalescence happens in one step, leading to a final surface fraction that is only slightly above the minimal surface fraction x_{sphere}.

It makes a difference if two clusters undergo a grazing collision or a frontal collision with a zero-collision parameter. Therefore the collision parameters and angles between the velocity vectors of the colliding clusters influence the coalescence process, especially at the beginning. The collision parameter is the smallest distance between the centers of mass of the clusters when passing straight by each other without any interaction. Here, it is extrapolated from the velocity vectors at first contact of the clusters determined by the Stillinger criterion.[26] The collision angle is the angle between the velocity vectors of the centers of mass. All collision parameters and angles for the investigated events are listed in Table II. Since the coalescence events are taken from particle-growth simulations, they are therefore at different conditions such as different carrier-gas and cluster temperatures, amount of carrier gas, cluster sizes, etc. Even if the relative collision parameters (divided by the sum of the cluster radii, see Table II) of two events are similar, the collision angles may be different. Therefore, a comparison of the events in terms of the collision parameters is difficult, and it requires many more events in order to get reasonable statistics. We document the parameters in Table II. One can see that more realistic coalescence events, in the sense that they are taken from a complete growth simulation, are usually asymmetric with respect to cluster size and properties, as well as collision parameters and angles.

IV. DISCUSSION

In the case of the structured clusters we identify here, under nonadiabatic conditions, a distinct, noncontinuous, three-step coalescence process in which each step happens in a different thermal state and heat exchange with the carrier

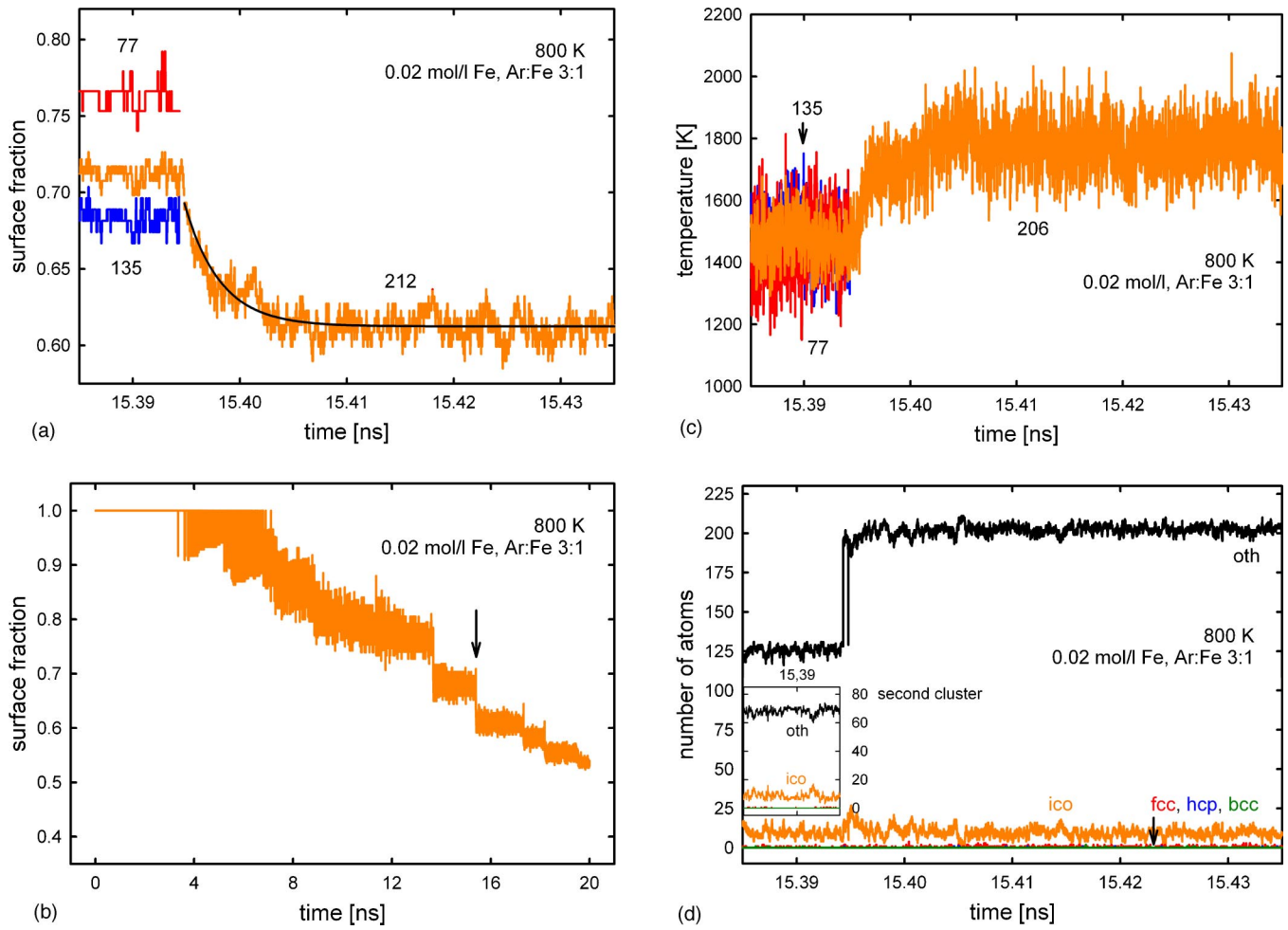

FIG. 6. (Color online) Results for the coalescence process *C*5. (a) The surface fraction of the clusters in high resolution. (b) The overall development of the surface fraction. The arrow marks the event shown in (a). (c) The temperature of the clusters and (d) common neighbor analysis of the clusters.

gas. The fast and sharp decrease of the surface fraction in the first few picoseconds after the collision of the two particles is related to the initial neck formation at the contact area of the particles. A similar behavior for the neck formation were described in MD simulations of the coalescence of Cu nanoparticles by Zhu and Averback.[29] Here we find that after this initial step the surface fraction remains nearly constant over a short period of time. This state corresponds to a dumbbell cluster as shown in Fig. 3(b). The second slower step, being the transformation from the dumbbell shape to an oval shape, happens on the order of hundreds of picoseconds of relaxation time. The final step in the coalescence from the oval shape towards the spherical shape is slowed down, because the difference in the surface energy, which is the driving force, is very low. Furthermore, the coalescence of solid clusters is based on the diffusion of atoms on the cluster surface, which is slow and hindered by edges acting as energy barriers.[7,30] Kinetic Monte Carlo simulations[31] revealed that the formation of a new layer requires the formation of a nucleus on an existing layer. This nucleus grows to a new layer, leading to a relaxation of the shape. In an investigation based on a continuum model it was found that there exists a limit on the facet size, beyond which shape relaxation is prohibited because of a high nucleation barrier.[32] This facet-size limit is about 1 nm, being on the order of magnitude of the clusters investigated here. The clusters which we obtained in our simulations have some defects in the surface as visible in Fig. 3(c). This is because the clusters do not contain the number of atoms required to fill the outer shell at collision. In addition the elevated cluster temperature increases the amount of defects. Therefore, one can expect that the coalescence process continues towards the spherical shape.

As a consequence, the last step of the coalescence can take orders of magnitude longer than the previous ones, and it is beyond the time scale of molecular simulations. Furthermore, the heat exchange between the cluster and the carrier gas is negligible in the first step of the coalescence process, which can therefore be regarded as quasiadiabatic. On the other hand, the heat exchange does affect the second coalescence step here. During the transition from the dumbbell to the oval structure the cluster temperature decreases continuously. The third step, leading to a spherical cluster, happens at the temperature level of the carrier gas and is therefore an isothermal process. The constant energy simulations of the coalescence of lead clusters by Hendy *et al.*[8] and silicon

clusters by Zachariah and Carrier[9] gave a similar sequence for the cluster shape. However, the effect of heat removal by a carrier gas was not included, which leads to a constant elevated temperature of the cluster, such as 50% above the initial temperature over a long period of time. The transitions from the dumbbell shape to the oval shape and especially from the oval to the spherical shape are affected by the heat removal and are therefore slower in the presence of a carrier gas than in a constant-energy ensemble. This leads to the three distinct and separate steps in the coalescence that differ not only in the cluster geometry and relaxation constants, but also in the heat exchange with the environment.

ACKNOWLEDGMENT

This work has been supported by the Ministry of Science and Research of North Rhine Westfalia within the joint project VerMoS.

*Email address: t.kraska@uni-koeln.de

[1] J. M. Montejano-Carrizales, M. P. Iniguez, and J. A. Alonso, J. Cluster Sci. **5**, 287 (1994).
[2] N. N. Lathiotakis, A. N. Andriotis, M. Menon, and J. Connolly, Europhys. Lett. **29**, 135 (1995).
[3] V. G. Grigoryan and M. Springborg, Phys. Chem. Chem. Phys. **3**, 5135 (2001).
[4] M. Pellarin, B. Baguenard, J. L. Vialle, J. Lerme, M. Broyer, J. Miller, and A. Perez, Chem. Phys. Lett. **217**, 349 (1994).
[5] W.A. de Heer, in *Metal Clusters at Surfaces*, edited by K.-H. Meiwes-Broer (Springer, New York, 2000).
[6] S. J. Zhao, S. Q. Wang, Z. Q. Yang, and H. Q. Ye, J. Phys.: Condens. Matter **13**, 8061 (2001).
[7] L. J. Lewis, P. Jensen, and J.-L. Barrat, Phys. Rev. B **56**, 2248 (1997).
[8] S. Hendy, S. A. Brown, and M. Hyslop, Phys. Rev. B **68**, 241403(R) (2003).
[9] M. R. Zachariah and M. J. Carrier, J. Aerosol Sci. **30**, 1139 (1999).
[10] F. H. Stillinger and T. A. Weber, Phys. Rev. B **31**, 5262 (1985).
[11] K. E. J. Lehtinen and M. R. Zachariah, Phys. Rev. B **63**, 205402 (2001).
[12] H. J. Freund and S. H. Bauer, J. Phys. Chem. **81**, 994 (1977).
[13] N. Lümmen and T. Kraska, Nanotechnology **15**, 525 (2004).
[14] N. Lümmen and T. Kraska, Comput. Mater. Sci. (to be published).
[15] M. S. Daw and M. I. Baskes, Phys. Rev. Lett. **50**, 1285 (1983).
[16] M. S. Daw and M. I. Baskes, Phys. Rev. B **29**, 6443 (1984).
[17] S. M. Foiles, M. I. Baskes, and M. S. Daw, Phys. Rev. B **33**, 7983 (1986).
[18] E. Clementi and C. Roetti, At. Data Nucl. Data Tables **14**, 177 (1974).
[19] R. Meyer and P. Entel, Phys. Rev. B **57**, 5140 (1998).
[20] J. D. Honeycutt and A. C. Andersen, J. Phys. Chem. **91**, 4950 (1987).
[21] A. S. Clarke and H. Jónsson, Phys. Rev. E **47**, 3975 (1993).
[22] C. L. Cleveland, W. D. Luedtke, and U. Landman, Phys. Rev. B **60**, 5065 (1999).
[23] Y. Wang *et al.* (unpublished).
[24] C. P. Poole, Jr. and F. J. Owens, *Introduction to Nanotechnology* (Wiley-Interscience, New York, 2003).
[25] W. Koch and S. K. Friedlander, J. Colloid Interface Sci. **140**, 419 (1990).
[26] F. H. Stillinger, J. Chem. Phys. **38**, 1486 (1963).
[27] A. Giesen, A. Kowalik, and P. Roth, Phase Transitions **77**, 115 (2004).
[28] *Handbook of Chemistry and Physics*, 72nd edition, edited by David R. Lide (CRC Press, Boca Raton, 1991).
[29] H. Zhu and R. S. Averback, Philos. Mag. Lett. **73**, 27 (1996).
[30] J. Krug, P. Politi, and T. Michely, Phys. Rev. B **61**, 14 037 (2000).
[31] N. Combe, P. Jensen, and A. Pimpinelli, Phys. Rev. Lett. **85**, 110 (2000).
[32] W. W. Mullins and G. S. Rohrer, J. Am. Ceram. Soc. **83**, 214 (2000).